Atmospheric Research 185 (2016) 84–91

Contents lists available at ScienceDirect

Atmospheric Research

journal homepage: www.elsevier.com/locate/atmosres

A new narrow-beam, multi-frequency, scanning radiometer and its application to in-flight icing detection

David J. Serke[a,*], Kimberly A. Reed[b,a], James Negus[b], Levi Blanchette[b], Randolph Ware[b,a], Patrick C. Kennedy[c]

[a]National Center for Atmospheric Research, Research Applications Laboratory, PO Box 3000, Boulder, CO 80307,USA
[b]Radiometrics Corporation, 4909 Nautilus Ct N, Suite #110, Boulder, CO 80301,USA
[c]CSU-CHILL Radar, 30750 Weld County Road 45, Greeley, CO 80631,USA

ARTICLE INFO

Article history:
Received 15 August 2016
Received in revised form 20 October 2016
Accepted 24 October 2016
Available online 26 October 2016

Keywords:
In-flight icing
Supercooled liquid water
Aviation hazard
Icing detection and avoidance
Microwave radiometer
Terrain mapping

ABSTRACT

A one degree beamwidth, multi-frequency (20 to 30 and 89GHz), dual-polarization radiometer with full azimuth and elevation scanning capabilities was built with the purpose of improving the detection of in-flight icing hazards to aircraft in the near airport environment. This goal was achieved by collocating the radiometer with Colorado State University's CHILL polarized Doppler radar and leveraging the similar beamwidth and volume scan regiments of the two instruments. The collocated instruments allowed for the liquid water path and water vapor measurements derived from the radiometer to be merged with the radar moment fields to determine microphysical and water phase characteristics aloft. The radiometer was field tested at Colorado State University's CHILL radar site near Greeley, Colorado during the summer of 2009. Instrument design, calibration, and initial field testing results are discussed in this paper.

1. Introduction

Aircraft accrete ice in flight when the cold surface of the aircraft comes into direct contact with supercooled liquid water. Accretion often occurs on engine intakes or propellers, leading edges of the wings, and tail fin structures. This in-flight icing can result in significant loss of aerodynamic performance due to increased drag, changes in the effective wing shape, and added weight. Loss of performance can lead to dangerous aircraft responses that are outside the realm of normal flight operations. Supercooled large drops, which are defined as those with a diameter greater than 50 μm, can freeze on aircraft structures unprotected or inadequately protected by anti-icing systems (Lynch and Khodadoust, 2001). Several episodes of aircraft icing have been related to the existence of supercooled large drops (Fernández-González et al., 2014a). As a result, the aviation safety community is dedicated to understanding aircraft icing detection with an overarching goal of accurately quantifying the presence of in-flight icing hazards on both a temporal and spatial scale (Barbagallo, 2015). Due to the need for an aircraft to be present in order to physically generate in-flight icing, the phenomena cannot be directly observed or measured with a remote sensing system. Ideally, all aircraft would be equipped with in-flight icing remote detection instrumentation that would provide detailed route-specific icing information, however budgetary constraints and technology shortfalls limit the practicality of this option. Therefore, a ground-based system with the capability to provide icing information to all aircraft entering and departing a terminal area is a key element in facilitating icing detection and avoidance.

Current techniques for remote detection and measurement of icing conditions generally rely on the identification of liquid water and the measurement or inference of the surrounding air temperature. Quasi-vertical profiles of supercooled liquid water content have been collected with vibrating wire sondes attached to standard meteorological radiosondes (Serke et al., 2014). These sondes have shown promise in accurately detecting supercooled water contents when compared to radiometers and research flight data, but are relatively expensive and provide only temporal snapshots of the atmospheric profile. The National Weather Service's network of polarized WSR-88D Doppler Radars operate at a wavelength of 10.7 cm. This wavelength is good at detecting precipitation-sized particles, but not cloud-sized particles such as small homogeneous

* Corresponding author.
E-mail addresses: serke@ncar.edu (D. Serke), k.reed@radiometrics.com (K. Reed), james.negus@radiometrics.com (J. Negus), l.blanchette@radiometrics.com (L. Blanchette), randolph.ware@radiometrics.com (R. Ware), pat@chill.colostate.edu (P. Kennedy).

http://dx.doi.org/10.1016/j.atmosres.2016.10.016

Fig. 1. Image of the NNMSR located at the CSU CHILL radar site during the summer of 2009.

supercooled liquid drops. These radars send pulses of energy radially outward and some fraction of the original power is returned to the radar receiver based on the sixth power of the diameter of the particles in the targeted sampled volume. This means that even large numbers of relatively smaller supercooled drops that coexist with small numbers of typically larger ice-phase crystals can be very difficult to detect (Ikeda et al., 2009). The Current Icing Product (CIP), developed by the National Center for Atmospheric Research (Bernstein et al., 2005) and currently in operational use by the FAA, ingests near real-time Rapid Update Cycle model output of atmospheric and microphysical conditions along with visible and infrared satellite data, surface weather observations, PIlot REPorts (PIREPs), and lightning network data to infer the presence of liquid along with subfreezing temperatures aloft. Another numerical weather prediction model approach for the forecasting of in-flight icing was detailed in Lamraoui et al. (2015). The NASA Icing Remote Sensing System (NIRSS) (Reehorst et al., 2006) makes use of the aviation hazard detection capabilities of several pieces of ground-based instrumentation. NIRSS consists of a vertically pointing Metek K-band radar used to define cloud top and base heights as well as determine cloud layer structure. In addition, there is a Radiometrics Corporation multi-frequency microwave radiometer (Solheim et al., 1998), that utilizes multiple channels to derive integrated liquid water and atmospheric temperature profiles. A laser ceilometer is also incorporated to further assist in cloud base detection. Software integrates the data streams in real-time, and the derived liquid is distributed within the detected cloud layer(s) based on internal logic in order to arrive at an in-flight icing hazard categorized risk assessment. This testbed system is an effort to provide in-flight icing hazard warnings with existing, cost-effective technologies. The system is currently positioned near John Hopkins Airport at the NASA Glenn Research Center in Cleveland, Ohio. Campos et al. (2014) utilized a method to detect the water phase dynamics of mixed-phase winter storms and applied the method to several winter cases. These results were

Table 1
NASA Narrow-beam Multi-channel Scanning Radiometer (NNMSR) specifications.

Parameter	NASA Narrow-beam Multi-channel Scanning Radiometer (NNMSR)
Frequency channels [GHz]	22.000, 22.234, 22.500, 23.000, 23.034, 23.500, 23.834, 24.000, 24.500, 25.000, 25.500, 26.000, 26.234, 26.500, 27.000, 27.500, 28.000, 28.500, 29.000, 29.500, 30.000, 89.0V, 89.0H
Antenna beamwidth	1°
Calibration	Microwave Ambient Target, Microwave LN2 Target, Terrain Mapping
Mass	Scanhead ~ 90 kg, Tripod ~ 16 kg
Dimensions	Scanhead 1 m × 1 m × 1.5 m, Tripod 3 m × 3 m × 2 m
Power consumption	110 V

compared to output from a ground-based instrumentation platform similar to NIRSS.

Combining ground-based microwave radiometer data with radar retrievals has shown great promise, however deficiencies with the current generation of radiometers have somewhat limited their capabilities. Among these shortcomings is an observation discontinuity problem resulting from the wide 6° beamwidth associated with the radiometer, which limits the spatial resolution and possibility of direct comparisons with the 1° beamwidth data available from weather surveillance radars.

Through previous efforts, solutions have been determined to resolve several technical challenges, including those mentioned above, with the design of a new instrument. The new instrument, referred to as the NASA Narrow-beam Multi-waveband Scanning Radiometer (NNMSR), is designed to operate in conjunction with and complementary to weather surveillance radars. This paper will detail the design (Section 2.1), calibration (Section 2.2), and overview of NNMSR data interpretation (Section 3), as well as field testing results of the NNMSR at Colorado State University's polarized CHILL S-band radar facility (Fig. 1) for the application of improving in-flight icing hazard detection and avoidance. This new instrument has the ability to provide the necessary information to fulfill the need for airport terminal area icing hazard warnings, when integrated into the existing NIRSS system and positioned in close proximity to the dual-polarization NEXRAD radars near each large national terminal.

The system also presents the possibility for additional applications beyond the scope of terminal area in-flight icing hazard detection and avoidance. One potential application includes the use of the system for decision support assistance in determining the need for deicing treatment in advance of aircraft departure via nowcasting. The inclusion of high-resolution icing information in the decision

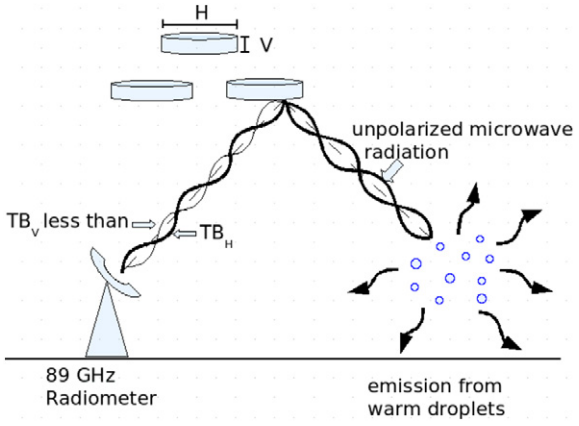

Fig. 2. Schematic of unpolarized microwave radiation becoming polarized and the resultant dual-polarization brightness temperature differences.

Table 2
Specifications for similar microwave radiometer instruments.

Parameter	Radiometrics MP-3000A Series Radiometer	Radiometer Physics RPG HATPRO-G4 Series Radiometer
Frequency channels	21 K-Band (22 to 30 GHz) channels 14 V-Band (51 to 59 GHz) channels	7 K-Band (22 to 32 GHz) channels 7 V-Band (51 to 58 GHz) channels
Antenna beamwidth	3–6°	3–6°
Calibration	Microwave Ambient Target Microwave LN_2 Target	Microwave Ambient Target Microwave LN_2 Target
Scanhead mass	~ 60 kg	~ 60 kg
Scanhead dimensions	63 cm × 36 cm × 90 cm	63 cm × 36 cm × 90 cm
Power consumption	110 V	90–230 V, 50 to 60 Hz

making process could in turn lead to substantial cost savings and a reduction in delays during inclement weather. Furthermore, the system has the ability to provide high-resolution mesoscale meteorological observations that could be used as valuable inputs for data assimilation in weather and climate models (Fabry and Meunier, 2009). Another potential non-weather related application includes terrain mapping in low visibility conditions, which will be briefly discussed in the calibration section.

2. Radiometer development

2.1. Design

The NNMSR was the product of a Small Business Innovation Research contract awarded to the Boulder, CO based Radiometrics Corporation in 2004. The goal of the contract was to design and construct a turnkey, fast-sampling, multi-frequency, dual-polarization, narrow beam radiometer system. The specified system was to include 21 channels in the K-band (22–30 GHz) as well as a separate dual-polarization W-band (89 GHz) receiver (Table 1). With its broad K-band sampling capability, the system can retrieve integrated water vapor along the observational path and provide information on the discrimination of liquid and ice phase hydrometeors by utilizing the W-band polarization information. The liquid water path can then be derived by combining data from both frequency bands. In addition, the instrument's fast beam steering system employs full range elevation and azimuth scanning capabilities resulting in the ability to operate simultaneously with a collocated weather surveillance radar. The beamwidth matching combined with the pointing capabilities demonstrate the importance of this technology as it allows for significantly enhanced observational retrievals as the radiometric observations provided by the NNMSR can be directly matched to the sample volume of radar observations. The combination of these measurement and pointing capabilities allows for the potential to provide terminal area icing hazard detection and warning for avoidance.

The K-band receiver was chosen for inclusion in the NNMSR because the frequency range includes the peak and adjacent off-peak region of the water vapor absorption line. By comparing the retrieved brightness temperatures (Tb) from a channel near the peak of the water vapor absorption line to a second channel in the water vapor window region, values for integrated water vapor and integrated cloud liquid water can be obtained. This information can be retrieved due to the idea that channels near the peak of the water vapor absorption line have an absorption coefficient that is nearly independent of altitude for water vapor. Channels well away from the absorption peak are utilized because the retrieved Tb is dominated by the absorption and emission from liquid water, which increases with the frequency squared.

The W-band channel is not only sensitive to cloud liquid water but is also strongly affected by microwave scattering patterns resulting from precipitation-sized glaciated hydrometeors (Troitsky et al., 2003). Small spherical hydrometeors, such as supercooled liquid water particles, radiate in an isotropic pattern resulting in nearly equal scattering in all directions (Fig. 2). This scattering pattern produces an unpolarized signal as both the horizontal and vertical axes are radiating equally. As particles grow larger, the scattering properties change with the changing mass. One microphysical response in the presence of supercooled liquid water is the rapid growth of dendritic crystal populations. These glaciated hydrometeors, no longer constrained by spherical dimensions, tend to take on oblate shapes such as dendrites. Such particles are inclined to fall with the largest axis oriented horizontally. This leads to greater scattering in the horizontal plane than the vertical plane when viewed from the surface resulting in a polarized retrieval signature (Fig. 2). For this reason, the W-band receiver was separated into vertically and horizontally polarized receiver channels in an attempt to differentiate cases where horizontally-oriented glaciated particles were present.

2.2. Comparison to other radiometers

Other similar commercially available, ground-based, passive microwave radiometers (Table 2) are compared to the specifications of the NNMSR. The current NNMSR version is both larger and about

Fig. 3. Image of the NNMSR with the Flatirons rock formations used for calibration in the background.

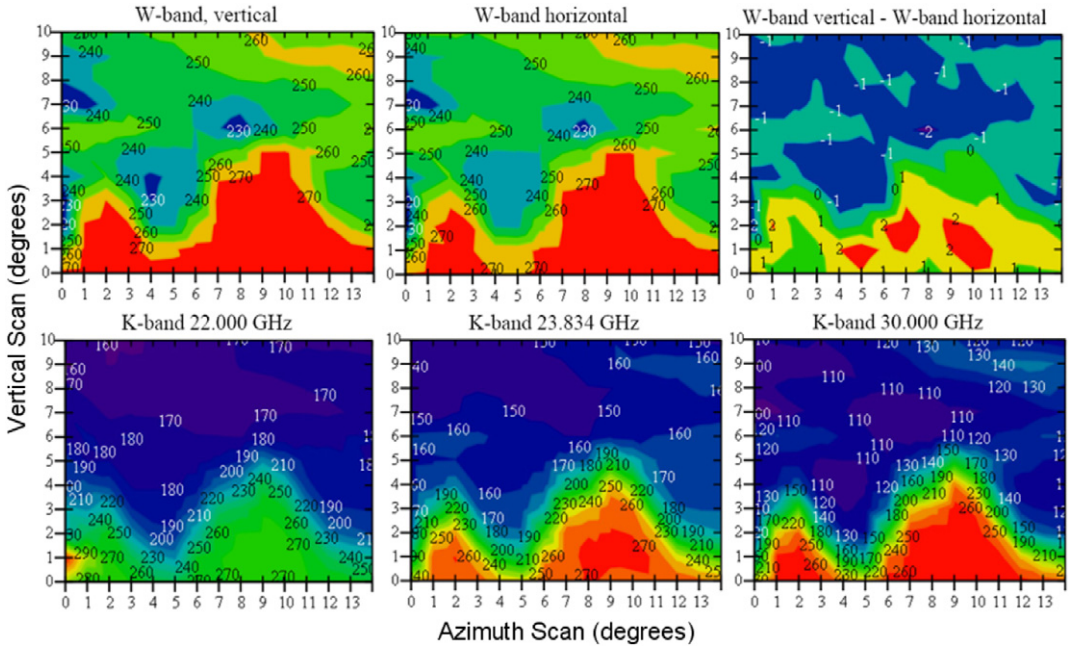

Fig. 4. 89.0GHz vertical (top left), 89.0GHz horizontal (top middle), 89.0GHz vertical minus horizontal (top right), 22.000GHz (bottom left), 23.834GHz (bottom middle), and 30.000GHz (bottom right) retrievals collected while scanning the Flatiron rock formations during the beam matching calibration.

50 percent heavier than these other instruments. Both the MP-3000A and the HATPRO instruments have multiple K- and V-Band channels for liquid, vapor, and temperature profiling. The main differences between the NNMSR and these other instruments include the refined one-degree beamwidth capability for higher resolution retrievals and the ability to calibrate via terrain mapping. In addition, the inclusion of the polarized W-band channels, which allows for qualitative discrimination of horizontally and vertically anisotropic from round particles, provides more information toward the detection of in-flight icing from non-icing environments.

2.3. Calibration

Initial calibration of the NNMSR was conducted at the Radiometrics Facility in Boulder, CO. Calibration parameters for each of the two receivers were determined using a hot and cold target, which consisted of an ambient temperature microwave absorber and a liquid nitrogen target respectively. All factory calibrations were conducted in an environmental chamber, which allowed for thermal stability and provided a dynamic ambient temperature range.

Following the factory calibration, the instrument was positioned to observe the Flatirons rock formations along the eastern slope of Green Mountain on the Front Range near Boulder, CO, approximately 7 km from the radiometer (Fig. 3). Elevation and azimuth beam-matching between the K- and W-Band radiometers was achieved by scanning a 1° by 1° grid encompassing the tallest peaks in the field of view. Multiple hours of vertical and horizontal profiles across the mountain targets were averaged and analyzed to ensure precise vertical and horizontal beam matching was achieved. Successful calibration resulted in collinear beams that matched the antenna gain pattern of NEXRAD and other weather research radars.

This radiometer beam matching calibration exercise unexpectedly demonstrated the capability of the radiometer to map terrain using multiple frequencies. The 24 and 30 GHz K-Band frequencies were particularly effective at mapping the terrain details in dry conditions as seen in Fig. 4. Following a light precipitation event during the calibration period, the 89 GHz dual-polarization retrievals demonstrated clear differences between the two orientations (Fig. 4).

3. Data interpretation

Crewell and Löhnert (2003) conducted a study that utilized a large dataset of radiosonde profiles to model clouds using three differing

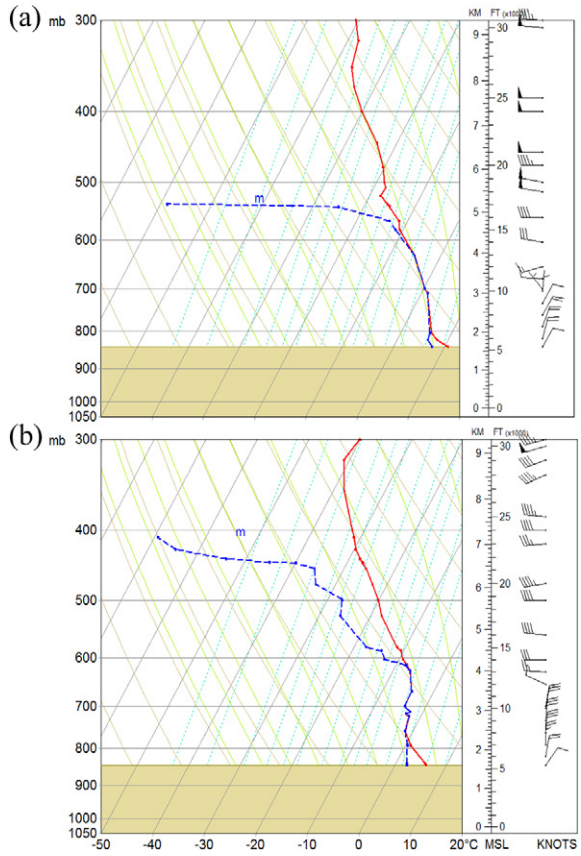

Fig. 5. Atmospheric profiles of ambient temperature and dew point temperature from 12 UTC 21 September 2009 (a) and 00 UTC 22 September 2009 (b) from Denver, Colorado.

cloud models. These models included a thresholding method, gradient method, and cloud microphysical model, all of which included modified adiabatic assumptions and relative humidity thresholding. Through this research, nine distinctive liquid water path (LWP) regression algorithms for multi-frequency ground-based radiometers were developed and applied to datasets in which clouds were generated using the three cloud models. The generalized form of this regression algorithm can be seen in Eq. (1), where c is the coefficient vector with dimensions defined by the number of retrieval frequencies used to collect the Tb observations.

$$LWP = c_0 + c^{*}Tb \tag{1}$$

The LWP regression algorithm for this study was selected based on availability and proximity of the NNMSR channels to those in the reference publication. The chosen algorithm demonstrated a 19.8 gm^{-2} RMS and 0.96 COR^2 between the modeled and retrieved profiles. The study determined that the inclusion of the W-Band retrievals made significant improvements in the resulting LWP correlation statistics. As a result of these findings, the LWP calculations for this study will include the W-Band retrieval information. Eq. (2) shows the algorithm used for this analysis.

$$LWP = c_0 - 7.5^{*}Tb_{23.0} + 6.6^{*}Tb_{28.5} + 4.5^{*}Tb_{90.0} \tag{2}$$

An important caveat of the NNMSR to note is that the presence of liquid water on the parabolic antenna in the field of view can result in artificially high Tb values, which in turn lead to incorrect LWP retrievals. However, the case study analyzed for this paper did not involve any precipitation reaching the surface and therefore no erroneous data were collected. In cases where precipitation does reach the surface, it is likely that the effects on Tb from the NNMSR platform would be significantly reduced when compared to similar Tb from an MP-series 'mailbox' radiometer due to the fact that an MP-series is viewing through a radome which acts to disperse focus from the lense. Several previous works detail the effects of freezing precipitation on Tb and LWC from MP-series radiometers (Woods et al., 2005;Fernández-González et al. 2014b). The NNMSR, with its downward looking receiver which is protected from precipitation accumulation, is viewing the radiation off of the canted reflector and should therefore mitigate any surface precipitation effects. A good

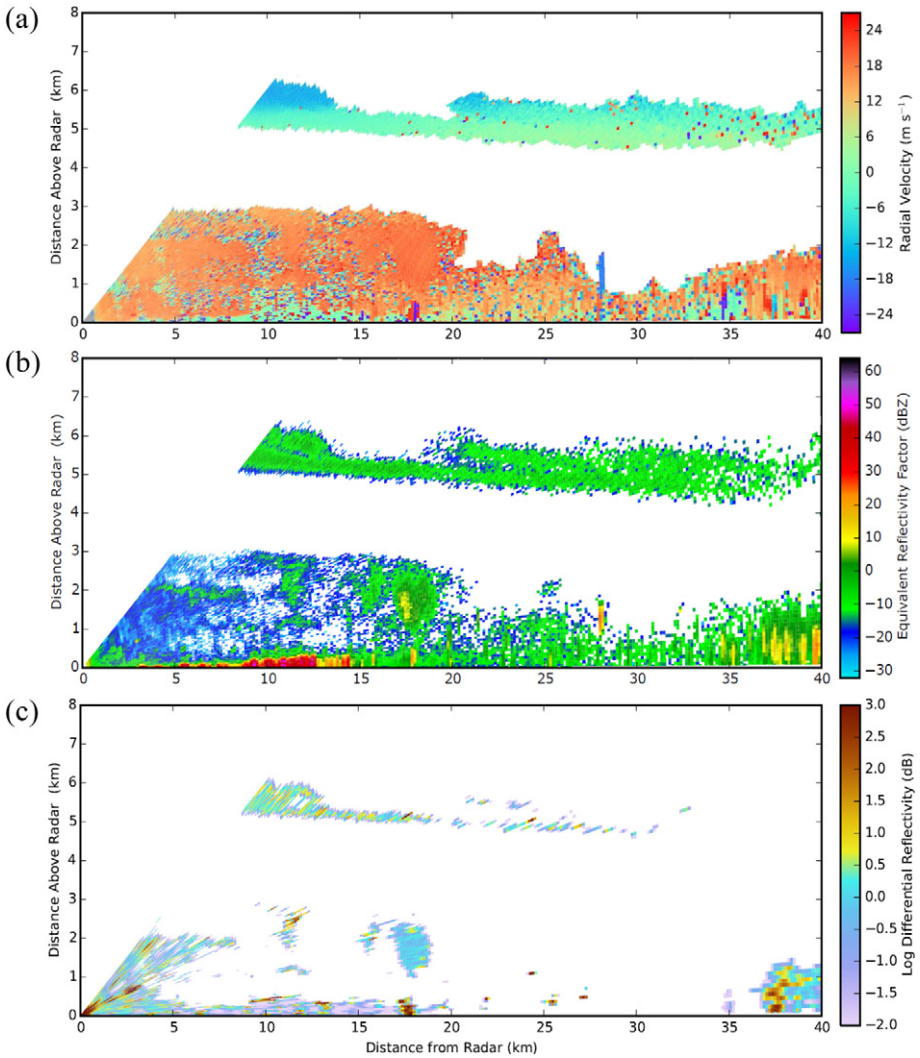

Fig. 6. Radial velocity (a), reflectivity (b), and differential reflectivity (c) retrievals from 175° azimuth CHILL RHI at 18:00 UTC 21 September 2009.

future experiment would be to spray water on the radome of an MP-series and the reflector of the NNMSR to compare the resulting Tbs. As the focus of this paper is to discern the usefulness of the new NNMSR during known in-flight icing conditions, this comparison will be left to a follow-on study.

4. Case study

The following case study elucidates how the NNMSR system can be used in conjunction with the polarized S-Band radar data to detect in-flight icing hazards in the airport operational environment.

On 21 September 2009, a moderate surface cold front originating from Canada propagated southward over the CHILL radar site, which is located in northeastern Colorado. Fig. 5 demonstrates the progression of the frontal system via consecutive radiosonde observations from the Denver launch facility located approximately 96 km south southwest of the radar site. Pre-frontal atmospheric conditions from 12 UTC on 21 September can be seen in Fig. 5a, which shows surface temperatures above 10 °C with a freezing level height near 1.6 km AGL and a saturated layer between 600 and 800 hPa. Cloud top temperature is approximately −10 ° C. Northerly winds from 0–1.5 km are also present with moderate westerly winds aloft. Fig. 5b shows the post-frontal environment at 00 UTC on 22 September characterized by a notably lower freezing level near 0.9 km AGL with cooler and drier conditions near the surface accompanied by a deep layer of northerly winds as the continental airmass is advected over the region. Moderate moistening occurs in the mid-levels as the surface cold front undercuts the warmer air forcing it to rise, cool, and condense, resulting in ideal conditions for supercooled cloud droplet formation. PIREPs received within 100 nm of the CHILL radar site (not shown), including four reports of moderate icing and one report of light icing from the associated time period, support the assertion of the presence of supercooled liquid. All icing reports corresponded to an altitude range between 4 km and 8 km, well above the freezing level.

At the time of the frontal passage near 18 UTC on 21 September, the scan strategy for the CHILL radar focused on range-height indicator (RHI) scans encompassing elevation angle heights between 1° and 30° at an azimuth angle of 175°, or nearly due south. The synoptic front, characterized by northerly low-level winds (red-toned colors), is clearly depicted in the radial velocity signature shown in Fig. 6a with winds flowing away from the radar in the lowest 3 km effectively advecting colder, denser air into the region while mid-level winds demonstrate a southerly component (blue-toned colors). Very low reflectivity values (negative dBZs in Fig. 6b) observed during the same scan in a layer between 4–7 km are consistent with findings from Serke et al. (2008), which indicated the presence of higher liquid water content during the cold season in regions of reflectivity gaps and reflectivity depressions characterized by very low dBZ values. Multiple concurrent commercial icing PIREPs suggest the presence of supercooled liquid in this upper cloud layer.

Another indicator of the existence of supercooled liquid is the retrieval of differential reflectivity (ZDR) values from zero to slightly positive such as those seen between 4–6 km in Fig. 6c. Values from zero to slightly positive indicate the vertical and horizontal axial dimensions of the targets in the viewing volume are similar, which is consistent with rounded particles such as those characteristic of supercooled liquid water.

In summary, the presence of supercooled liquid water during this event was detected via the CHILL radar's polarized moments and with multiple icing PIREP observations. These observations were combined to validate the radiometer retrievals, which are presented below.

Although the NNMSR in current form is unable to retrieve liquid ranging information, each pixel in the retrieval is representative

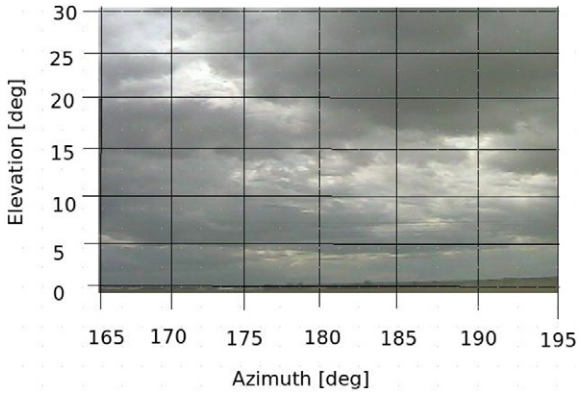

Fig. 7. Visual sky sector image from 18:04 UTC 21 September 2009 showing a stratocumulus cloud layer.

of the derived range-integrated LWP measurement. Together these pixels form a sector image of the region of the sky the instrument is focused on, similar to the visual view of the sky taken at 18:04 UTC from a collocated webcam (Fig. 7), which depicts a stratocumulus cloud layer. Fig. 8a shows the LWP field at 18:04 UTC derived from Eq. (2) and data from the NNMSR 14-minute scan centered at 180° azimuth or due south. Evidence of supercooled liquid can be seen in the horizontal bands of elevated LWP in excess of 600 gm^{-2} that are apparent between the 12° and 30° elevation angles. These banded regions coincide with areas of near zero V-H polarization differences

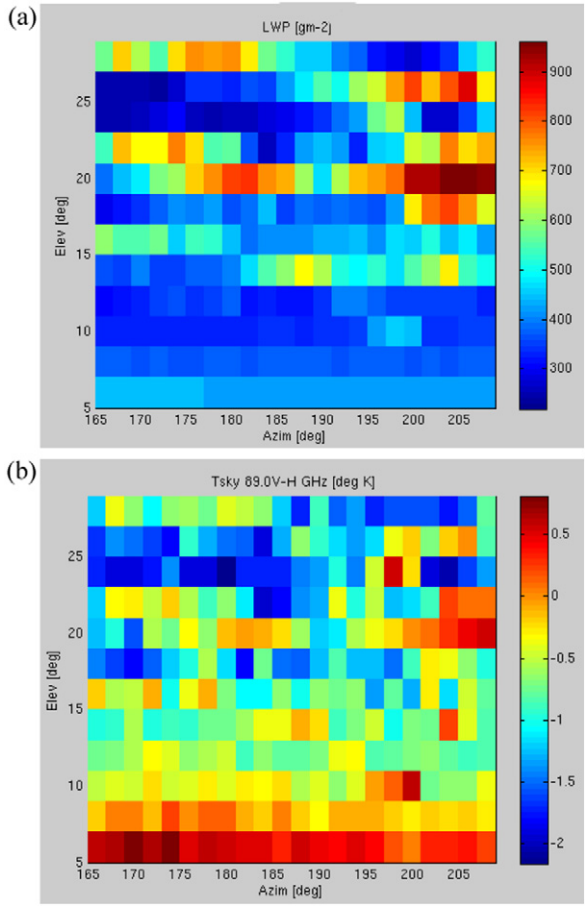

Fig. 8. NNMSR derived LWP [gm^{-2}] (a), and 89 GHz V-H Tb [K] (b) from 18:04 UTC 21 September 2009.

in the 89 GHz retrievals (Fig. 8b) suggesting isotropic scattering and small spherical particles such as supercooled liquid water drops.

The liquid water content (LWC) of the retrieval path can be determined using observed values obtained from both the CHILL and NNMSR retrievals. Given 800 gm^{-2} of LWP (Fig. 8a) distributed through the upper-cloud layer with a path length of 1500 m (Fig. 6b) at a slant angle of 20°, resulting calculations determine that 0.4 –0.5 gm^{-3} of LWC are dispersed throughout the cloud depth. This significant amount of LWC corresponds directly to the PIREP observations of *moderate* in-flight icing.

Four hours later, at 22:00 UTC, the radar and radiometer remained operational utilizing the same scanning strategies as those previously discussed. Radial velocity radar retrievals indicated northerly flow from the cloud base at 1 km AGL up to 5 km AGL (red-toned colors) (Fig. 9a), which is consistent with a stable post-frontal deepening layer of cold air. This stable layer is evident in the visual view of the sky in Fig. 10, characterized by a uniform stratus cloud deck. Fig. 9b shows virtually all CHILL reflectivity retrievals greater than 0 dBZ with a sizable region above 10 dBZ, indicating a significant increase in mean particle diameter. It is important to note that the lowest cloud layers have above freezing temperatures (as noted in Fig. 5b) as evidenced by a brightband in the radar moments due to melting snow falling below the zero degree isotherm. Vertical streamers near the surface indicate hydrometeors are falling below the cloud base, however a lack of continuation to the surface suggests dry conditions are dominating, leading to sublimation before the precipitation reaches the ground. ZDR values near +1 dB at cloud base and cloud top indicate the presence of particles with a horizontally polarized signature suggesting larger glaciated hydrometeors (Fig. 9c). When combined, these retrieval characteristics are indicators of the transition from the pre-frontal presence of supercooled liquid water aloft to that of a fully glaciated post-frontal particle population. This evidence of glaciated hydrometeors is supported by the lack of PIREPs reporting in-flight icing during a time of day

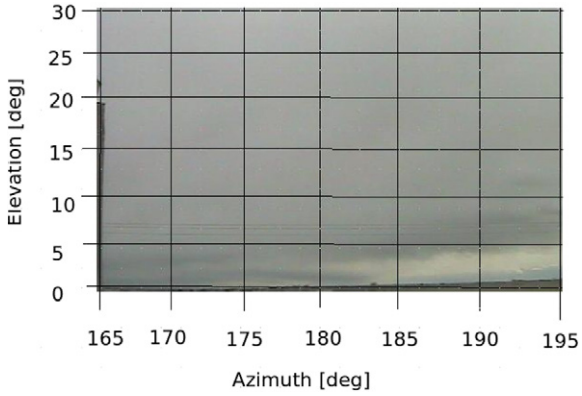

Fig. 10. Visual sky sector image from 22:28 UTC 21 September 2009 showing a uniform stratus cloud deck.

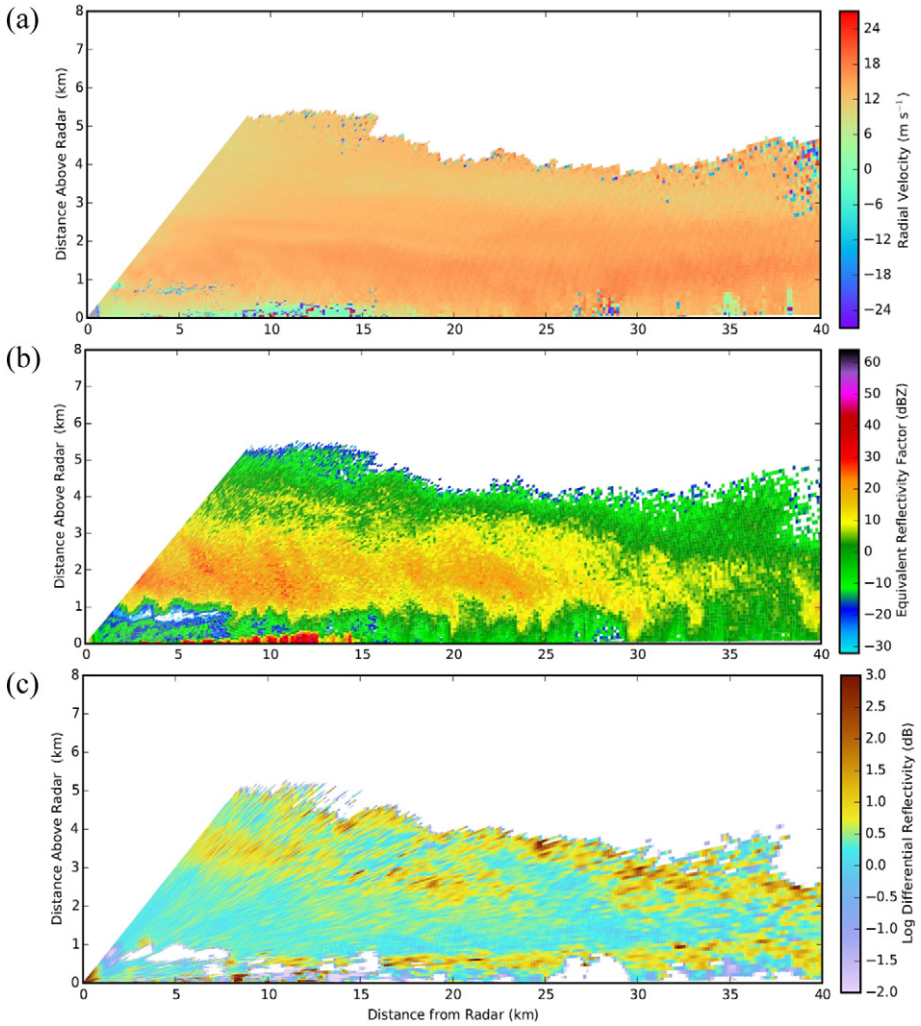

Fig. 9. Radial velocity (a), reflectivity (b), and differential reflectivity (c) retrievals from 175° azimuth CHILL RHI at 22:04 UTC 21 September 2009.

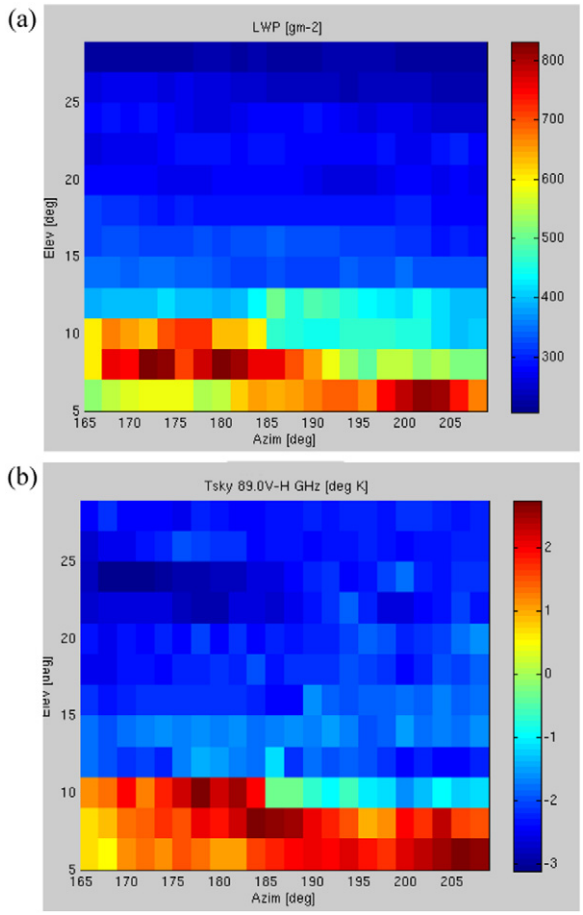

Fig. 11. NNMSR derived LWP [gm^{-2}] (a), and 89 GHz V-H Tb [K] (b) from 22:28 UTC 21 September 2009.

when a significant volume of air traffic was transecting the region of interest.

Post-frontal observations from the NNMSR show retrieved LWP values well below 400 gm^{-2} in the same azimuth region between the 12° and 30° elevation angles (Fig. 11a), indicating a significant decrease in the amount of supercooled liquid water present. The 89 GHz V-H dual-polarization signatures at the corresponding elevation angles above 12° suggest the presence of horizontally oriented glaciated hydrometeors as depicted by negative polarization differences (Fig. 11b). Closer to the surface, both the LWP and dual-polarization NNMSR observations exhibit elevated retrieval values. Theoretical calculations by Troitsky et al. (2003) demonstrate that polarization differences at 85 GHz become large and positive at low viewing angles in the presence of horizontally oriented oblate particles such as plates, dendrites, or rods. The NNMSR retrievals combined with the slightly positive ZDR values from the radar and findings from previous research confirm the presence of small horizontally oriented glaciated hydrometeors.

5. Summary

In an effort to provide in-flight icing hazard and detection in an airport terminal area, the dual-frequency, dual-polarization NASA Narrow-beam Multi-waveband Scanning Radiometer was developed to allow for collocated beam-matching with weather surveillance radar retrievals. Following two months of field-testing and data collection alongside the CSU CHILL Radar, the newly designed, remotely operated NNMSR demonstrated exceptional receiver stability and mechanical functionality.

Case study data collected during the test period demonstrated the ability of the NNMSR to aid in in-flight icing hazard detection. Calculated liquid water path values from the K-Band receiver combined with dual-polarization retrievals from the W-Band receiver allowed for the positive identification of spherical liquid hydrometeors. The presence of supercooled liquid was confirmed using remotely sensed radar moment information combined with pilot reports of *light* to *moderate* in-flight icing conditions.

Based on the system stability and case study results, it was determined that the NNMSR would be a valuable addition to NIRSS for detecting in-flight icing hazards in the airport environment particularly when co-located with dual-polarization weather surveillance radars such as those in the terminal doppler weather radar and NEXRAD networks.

Acknowledgments

This work was done under the NASA Transformative Aeronautics Concepts Program and the NASA Aviation Safety Research Program. The National Center for Atmospheric Research is sponsored by the National Science Foundation. Any opinions, findings, and conclusions or recommendations expressed in this publication are those of the author(s) and do not necessarily reflect views of the National Science Foundation.

References

J., Barbagallo, 2015. USDOT/FAA Advisory Circular: Pilot Guide: Flight in Icing Conditions.

B.C., Bernstein, F., McDonough, M.K., Politovich, B.G., Brown, T.P., Ratvasky, D.R., Miller, C.A., Wolff, G., Cunning, 2005. Current icing potential: algorithm description and comparison with aircraft observations. J. Appl. Meteorol 44, 969–986. http://dx.doi.org/10.1175/jam2246.1.

E.F., Campos, R., Ware, P., Joe, D., Hudak, 2014. Monitoring water phase dynamics in winter clouds. Atmos. Res. 147-148, 86–100. http://dx.doi.org/10.1016/j.atmosres.2014.03.008.

S., Crewell, U., Löhnert, 2003. Accuracy of cloud liquid water path from ground-based microwave radiometry 2. Sensor accuracy and synergy. Radio Sci. 38, 1–11. http://dx.doi.org/10.1029/2002RS002634.

F., Fabry, V., Meunier, 2009. Conceptualisation and design of a "mesoscale radiometer". 8th Int. Symp. Tropospheric Profiling 2–5.

S., Fernández-González, J.L., Sánchez, E., Gascón, L., López, E., García-Ortega, A., Merino, 2014a. Weather features associated with aircraft icing conditions: a case study. Sci. World J. http://dx.doi.org/10.1155/2014/279063.

S., Fernández-González, F., Valero, J.L., Sánchez, E., Gascón, L., López, E., García-Ortega, A., Merino, 2014b. Observation of a freezing drizzle episode: a case study. Atmos. Res. 149, 244–254. http://dx.doi.org/10.1016/j.atmosres.2014.06.014.

K., Ikeda, R.M., Rasmussen, E., Brandes, F., McDonough, 2009. Freezing drizzle detection with WSR-88d radars. J. Appl. Meteorol. Climatol. 48, 41–60. http://dx.doi.org/10.1175/2008JAMC1939.1.

F., Lamraoui, R., Benoit, J., Perron, G., Fortin, C., Masson, 2015. Hybrid fine scale climatology and microphysics of in-cloud icing: from 32 km reanalysis to 5 km mesoscale modeling. Atmos. Res. 154, 175–190. http://dx.doi.org/10.1016/j.atmosres.2014.11.006.

F.T., Lynch, A., Khodadoust, 2001. Effects of ice accretions on aircraft aerodynamics. Prog. Aerosp. Sci. http://dx.doi.org/10.1016/S0376-0421(01)00018-5.

A., Reehorst, M., Politovich, S., Zednik, G., Isaac, S., Cober, 2006. Progress in the development of practical remote detection of icing conditions. . NASA Tech. Rep.

D.J., Serke, F., Mcdonough, M.K., Politovich, 2008. Analysis of 3-d NEXRAD mosaic reflectivity data colocated with research aircraft and satellite data: implications on in-flight icing. 13th conf. Aviat. Range. Aerosp. Meteorol

D., Serke, E., Hall, J., Bognar, A., Jordan, S., Abdo, K., Baker, T., Seitel, M., Nelson, R., Ware, F., McDonough, M., Politovich, 2014. Supercooled liquid water content profiling case studies with a new vibrating wire sonde compared to a ground-based microwave radiometer. Atmos. Res. 149, 77–87. http://dx.doi.org/10.1016/j.atmosres.2014.05.026.

F., Solheim, J.R., Godwin, E.R., Westwater, Y., Han, S.J., Keihm, K., Marsh, R., Ware, 1998. Radiometric profiling of temperature, water vapor and cloud liquid water using various inversion methods. Radio Sci. 33, 393–404. http://dx.doi.org/10.1029/97RS03656.

A.V., Troitsky, A.M., Osharin, A.V., Korolev, J.W., Strapp, 2003. Polarization of thermal microwave atmospheric radiation due to scattering by ice particles in clouds. J. Atmos. Sci. 60, 1608–1620.

C.P., Woods, M.T., Stoelinga, J.D., Locatelli, P.V., Hobbs, 2005. Microphysical processes and synergistic interaction between frontal and orographic forcing of precipitation during the 13 december 2001 IMPROVE-2 event over the oregon cascades. J. Atmos. Sci. 62, 3493–3519. http://dx.doi.org/10.1175/JAS3550.1.